



*Supplement of*

## **How does integrating multi-scale monitoring and compound-specific isotope analysis improve the evaluation of *S*-metolachlor degradation in agroecosystems?**

**Boris Droz et al.**

*Correspondence to:* Boris Droz (drozditb@oregonstate.edu) and Sylvain Payraudeau (sylvain.payraudeau@engees.unistra.fr)

The copyright of individual parts of the supplement might differ from the article licence.

15	<b>Contents</b>	
16		
17	S1 Supplement methods. ....	3
18	S1.1 Catchment and sub-catchment delimitation.....	3
19	S1.2 Catchment description and <i>S</i> -metolachlor application dose scenario. ....	3
20	S1.3 Continuous sampling. ....	4
21	S1.4 Analytic methods.....	5
22	S1.5 <i>S</i> -metolachlor mass balance.....	6
23	S1.5.1 Estimation of the volatilization after application.....	6
24	S1.5.2 Estimation of <i>S</i> -metolachlor photodegradation in the Souffel river. ....	7
25	S1.6 Variation of <i>S</i> -metolachlor concentration in topsoil.....	7
26	S1.7 Averaged in-stream transit time and degradation within the river reach between A1 and A2. ....	10
27	S1.8 Stable isotope fractionation with increasing <i>S</i> -metolachlor in-stream transit time.....	10
28	S2 Supplement results. ....	12
29	S2.1 Area-normalized discharges. ....	12
30	S2.2 Wetness index.....	13
31	S2.3 <i>S</i> -metolachlor concentrations per location.....	14
32	S2.4 Detailed off-site transport of <i>S</i> -metolachlor per event.....	15
33	S2.5 Pesticide mass balance .....	16
34	S2.6 Hydrochemistry .....	18
35	S2.7 Wastewater treatment plant (WWTP) contribution .....	19
36	S2.8 <i>S</i> -metolachlor transformation products.....	21
37	S3 Supplement references.....	24
38		
39		

40 **S1 Supplement methods.**

41 **S1.1 Catchment and sub-catchment delimitation.**

42 The European Digital Elevation Model (EU-DEM, v1.1, <https://land.copernicus.eu>) with a 25 m resolution for the  
43 year 2011, along with the river network data (BD TOPO® 2019, <http://www.ign.fr>), was used to delineate the  
44 catchment and sub-catchments (Kwast and Menke, 2022), using an automatic procedure implemented in GRASS  
45 v.7.2.2 within R4.2.2 (package 'rgrass' v.0.3-6) at both automated and grab sampling locations. Briefly, water  
46 flow direction was calculated for each pixel using a depression elevation map. Next, water accumulation was  
47 determined by counting the number of adjacent pixels that drain through each pixel. Finally, the catchment was  
48 delineated using the drainage direction and the sampling location, which serves as the catchment's outlet point.

49

50 **S1.2 Catchment description and S-metolachlor application dose scenario.**

51 For each agricultural field, three S-metolachlor application scenarios were considered: the maximum legal dose  
52 (hereafter 'maximal'), a dose based on local farming recommendations (<https://alsace.chambre-agriculture.fr/>,  
53 hereafter 'economic'; Table S1), and a dose derived from farmer surveys (hereafter 'realistic'). Application rates  
54 for each field were calculated using data from Table S1. Soils in the catchment areas (<20 m depth), as identified  
55 by satellite remote sensing, were predominantly Cambisols (83%), followed by Luvisols (13%), with the  
56 following predicted properties: bulk density  $1.29 \pm 0.04 \text{ kg dm}^{-3}$ , clay  $21.6 \pm 1.9\%$ , silt  $45.9 \pm 3.6\%$ , and sand  
57  $32.5 \pm 4.3\%$  (Hengl et al., 2017).

58

59

60 **Table S1: Main crop types and S-metolachlor application at the Souffel catchment in 2019.**

Field	Crop type (%) <sup>a</sup>	S-metolachlor application ( $\text{g ha}^{-1} \text{ yr}^{-1}$ )		
		Maximal <sup>b</sup>	Economic <sup>c</sup>	Realistic min-max <sup>d</sup>
Sugar beet	10.4	576	384	576 – 672
Corn	49.7	1920	1280	160 – 1000
Wheat	21.9			
Others cereals	1.4		no application	
Meadow	4.6			
Vegetable (zucchini, pumpkin, squash, beans)	0.2	1500		not in survey
Soja / sorgho / sunflower	0.2	1344		
Divers (tabaco, hops,...)	11.6		no application	

61 <sup>a</sup> Calculated from the Registre Parcellaire Graphique ([www.ign.fr](http://www.ign.fr)) from 2019. S-metolachlor applications are  
62 reported and then applied based on field type (<https://ephy.anses.fr/>): <sup>b</sup> follow regulatory limits, <sup>c</sup> based on local  
63 farming recommendations (<https://alsace.chambre-agriculture.fr/>) and <sup>d</sup> based on survey results from the A2 sub-  
64 catchment.

65

66

67 **Table S2: Sub-catchment characteristics.**

Outlet of the catchment	A1	A2	A3
Size (km <sup>2</sup> )	2.3	3.6	115
Slope (%) <sup>a</sup>	n.m.	3.8 ± 1.2	2.4 ± 2.2
River length (km) <sup>a</sup>	0.7	2.2	73
Strahler order <sup>a</sup>	1	1	1–3
Farmland (%) <sup>a</sup>	91	93	87
Prop. wheat/corn/beets (%) <sup>b</sup>	36/25/3	32/31/12	22/50/10
Prop. wheat/corn/beets (%) <sup>c</sup>	28/20/2	27/26/4	n.m.

68 <sup>a</sup> from BD TOPO® 2017, www.ign.fr.69 <sup>b</sup> Registre Parcellaire Graphique 2019, www.ign.fr.70 <sup>c</sup> from survey.

71 n.m. not measured.

72

73 **S1.3 Continuous sampling.**74 **Table S3: Automatic water sampler characteristics, flow control and multiprobe devices.**

Loc.	Sampling	Capacity (mL)	Flow slaving control	Flow meter	Temp., pH, cond. <sup>a</sup>
A1	ISCO Avalanche	12 x 350	Doppler (ISCO 2150)	ISCO 2150	Ponsel ODEON
A2	ISCO Avalanche	12 x 350	Doppler (IJINUS VLI H/V)	IJINUS VLI H/V	HANNA HI 9289
A3	ISCO 6712	24 x 950	Bubbler flow module (ISCO 730)	VEGAPULS WL S 61	HANNA HI 9289
G1–9	Grab sampling	2000	None	OTT Nautilus C2000 / Sensa Z300	WTW multi 350i

75 <sup>a</sup>Temperature, pH and conductivity were measured every two minutes.

76

77 **Table S4: Rain gauge location and material.**

ID	Name	Location (WGS 84)	Material	Accuracy (mm)	Ref.
R1	LYHGES	48°40'03"N 7°34'51"E	Precis Mecanique mouvement 3030	0.2	A
R2	IALSACES11	48°37'48"N 7°37'12"E	Davis Vantage Pro2 Plus	0.2	B
R3	EMSVENDEN	48°40'18"N 7°42'42"E			C
R4	EMSMUNDOL	48°38'25"N 7°43'16"E			C
R5	EMSOBERHAUS	48°36'20"N 7°41'46"E	Precis Mecanique mouvement 3039/1	0.1	C
R6	EMSWOLFIS	48°34'47"N 7°40'20"E			C
R7	EMSHOLTZ	48°33'47"N 7°39'00"E			C
R8	IWASSELO8	48°38'27"N 7°27'00"E	Eurochron EC-4406126	n.s.	B
R9	IALSACEC18	48°40'48"N 7°34'48"E	Davis Vantage Vue	0.2	B

78 A data is available in Droz et al. (2025), B data were downloaded from www.wunderground.com/weatherstation  
79 and C data are provide by the city of Strasbourg.

80

81

82 **S1.4 Analytic methods.**83 **Table S5: Analytic methods description.**

<b>Water characterization</b>	<b>Methods in brief</b>	<b>Reference</b>
pH/conductivity/ temperature	Electrode measurement (pH/cond multi 350i, WTW).	
Water velocity	Handheld electromagnetic water flow meter (Nautilus C2000 / Sensa Z300, OTT).	
Total suspended solid (TSS)	Sample filtered with a bottle-top vacuum filtration unit through a glass filter (GF/5, 0.4 µm average pore size, Macherey-Nagel) and dried at room temperature in a desiccator.	Modified NF 872
Bulk density	Weigh a soil field sample that has a cylindrical known volume (48 cm <sup>3</sup> , core method).	ISO 11272
Dissolved organic carbon (DOC)/ dissolved inorganic carbon (DIC)	Sample is passed through a 0.25 µm cellulose acetate filter, then dissolved organic carbon is oxidized into CO <sub>2</sub> and detected by infrared spectrometry (TOC-V CPH, Shimadzu).	NF EN 1484
Iron (Fe <sup>2+</sup> , Fe <sup>3+</sup> )	Presence/absence of iron is measured by semi-quantitative strip (P/N 1.16982.0001, Reflectoquant®, Merck) with reflectometer (P/N 1.16970.0001, Merck). If present, UV-vis spectrophotometric measurement is made at 511 nm after reaction with 1,10-phenanthroline to form a red complex (P/N 1.00796.0001, Spectroquant®, Merck).	DIN 38406-1
Cations/anions (Na <sup>+</sup> , K <sup>+</sup> , Mg <sup>2+</sup> , Ca <sup>2+</sup> , NH <sub>4</sub> <sup>+</sup> , Cl <sup>-</sup> , NO <sub>3</sub> <sup>-</sup> , SO <sub>4</sub> <sup>2-</sup> , PO <sub>4</sub> <sup>3-</sup> )	Ion chromatography analysis (ICS-5000, Dionex/Thermo Fischer). Bromide can be measured if there is a low sulfate content.	US EPA 300.7/300.0
Nitrite (NO <sub>2</sub> <sup>-</sup> )	Presence/absence of nitrite is measured by semi-quantitative strip (P/N 1.16973.0001, Reflectoquant®, Merck) with reflectometer (P/N 1.16970.0001, Merck). If present, UV-vis spectrophotometric measurement is made at 536 nm after Reaction with <i>N</i> -(1-naphthyl)ethylenediamine dihydrochloride to form a red-violet azo complex (P/N 1.14776.0002, Spectroquant®, Merck).	DIN 26777
Minor element (Mn, Cu, Si, Al, Fe, Zn, Ti, P)	Sample filtered through 0.25 µm, digest 1 mL sample by HNO <sub>3</sub> (50 mL, 69%) and oxalic acid (50 mL, 1 M), aqueous phase measured by inductively coupled plasma-optical emission spectrometry (ICP-OES, ICAP6500, Thermo Fisher).	In house method
<b>Sediment characterization</b>		
Residual humidity (RH) content	Sample dried until constant mass at 105°C.	ISO 11465
pH <sub>H2O</sub> / pH <sub>CaCl2</sub>	Electrode measurement of 1:5 w/w sediment:water or 0.01 M CaCl <sub>2</sub> .	ISO 10390
Organic carbon (f <sub>OC</sub> ) / inorganic carbon (C <sub>inorg</sub> )	Total combustion by elementary analyzer (CHN, FLASH 2000 NC, Thermo Fisher). Prior to organic carbon measurement, sample was decarbonated by HCl fumigation: C <sub>inorg</sub> = total C - f <sub>OC</sub> .	ISO 10694, Ramnarine et al. (2011)
Particle size fraction (0.1 µm to 2 mm)	Sample was pre-treated with a proportion 1:3 (v/v) of H <sub>2</sub> O <sub>2</sub> at 60 °C to degrade organic matter, KCl 1:50 (v/v) or HCl 1:20 (v/v) was added if the sample contained carbonate or no carbonate respectively to extract flocculent cations and 1:1 (v/v) solution of Natrium hexametaphosphate 0.55% was added to disperse the particles. Measurement performed by laser granulometry in aqueous mode (LS230, Beckmann Coulter).	ISO 13320
Elementary analysis (Na, K, Mg, Ca, Ti, Mn, Fe, Al, Si)	Sample prepare by fusion alkaline with lithium tetraborate and analyzed by inductively coupled plasma-optical emission spectrometry (ICP-OES, ICAP6500, Thermo Fisher).	NF ISO 14869-2

85 The minimal change of isotope signature of the  $^{13}\text{C}$  ( $\Delta\delta^{13}\text{C}_{min}$ ), before which isotope fractionation can be  
 86 attributed to degradation, was determined as the propagation of uncertainties associated with measurements and  
 87 sample preparation (Alvarez-Zaldívar et al., 2018) and calculated as follow:

$$88 \quad \Delta\delta^{13}\text{C}_{min} = \sqrt{\sigma_{ea}^2 + \sigma_s^2 + \sigma_{au}^2} + \Delta\delta^{13}\text{C}_{ext} \quad (\text{S1})$$

89 where  $\sigma_{ea}^2$ ,  $\sigma_s^2$  and  $\sigma_{au}^2$  are the uncertainty associated with the triplicate measurement of the initial product by an  
 90 elemental analyzer IRMS (0.5‰ for C), the sample uncertainty associated with the triplicate measurement and  
 91 the maximal analytical uncertainty of the GC-IRMS (0.5‰ for C), respectively.  $\Delta\delta^{13}\text{C}_{ext}$  ( $-1.23 \pm 0.3\%$  and  $0.11$   
 92  $\pm 0.4\%$  for sediment and water respectively) is the trueness of the  $\delta^{13}\text{C}$  measurement associated with the  
 93 extraction procedure, as previously determined in Droz et al. (2021).

94

## 95 **S1.5 S-metolachlor mass balance.**

### 96 **S1.5.1 Estimation of the volatilization after application.**

97 Proportion of volatilization after application was estimated based on the semi-empirical physical based model  
 98 developed from Hippelein and McLachlan (2000) and generalized over 224 molecules including S-metolachlor  
 99 by Davie-Martin et al. (2013). Briefly, the model relies on a multiphase partitioning approach based on soil–air  
 100 ( $K_{soil-air}$ ) and water–air ( $K_{water-air}$ ) partition coefficients for the topsoil. Air temperature and moisture  
 101 combined with topsoil relative moisture and organic carbon content are the principal parameters accounting for  
 102 variation of the rate of the volatilization in the model, which was consistent with observations made in agricultural  
 103 fields (Gish et al., 2011; Prueger et al., 2005). The volatilization was only considered to take place for 36 h  
 104 following application as observed in the field (Gish et al., 2011; Prueger et al., 2005). Table S6 summarizes the  
 105 parameter values used in the model to calculate the volatilization after each reported application. The predicted  
 106 contribution of volatilization accounts for 2.2 to 5.5% mass loss of applied S-metolachlor within 36 h after the  
 107 application, which is consistent with the [ $^{14}\text{C}$ ]metolachlor experiment on unsaturated subsurface soils where  
 108 volatilization was less than 5% (Rice et al., 2002).

109

110 **Table S6: Local parameters used for the volatilization estimation.**

Parameter	Values	Reference
Temperature (min–max)	5.7–20.9°C	www.meteo-offenheim.fr
Relative humidity (annual average)	77%	www.meteo-offenheim.fr
Bulk density	1.29 kg L <sup>-1</sup>	Hengl et al. (2017)
Soil organic carbon	0–50%	Hengl et al. (2017)
Soil depth <sup>a</sup>	50 cm	Huang and Frink (1989)
Soil moisture	min–max 0–100% average: 28%	Bauer-Marschallinger et al. (2018)

111 <sup>a</sup> topsoil depth average where >80% of the S-metolachlor total amount in topsoil was found within 1-  
 112 2 weeks following application.

### 113 **S1.5.2 Estimation of *S*-metolachlor photodegradation in the Souffel river.**

114 The extent of *S*-metolachlor photodegradation was estimated as following Fono et al. (2006) and Schwarzenbach  
115 et al. (2016). The approach compares photodegradation rates obtained under solar simulator at 330 nm (Drouin et  
116 al., 2021) with conditions expected in the Souffel River.

117 First, water absorbance at 330 nm ( $A_{330}$ ) of Souffel river was estimated as similar as Fono et al. (2006) and follow:

$$118 \quad A_{330} = \log(I_0/I) = 1.3 \text{ (S2)}$$

119 where  $I_0$  is the incident light intensity emission of the UV-vis spectrometer and  $I$  the transmitted light at 330 nm.

120 Then, the depth of the photic zone ( $Z_{photic}$ ) in the Souffel River in m was estimated as follow:

$$121 \quad Z_{photic} = \frac{A_{330}}{\alpha_{330}} = 0.2 \text{ m (S3)}$$

122 where  $\alpha_{330}$  was the beam attenuation coefficient ( $6 \text{ m}^{-1}$  for muddy river water).

123 Then, the screening factor ( $S$ ) to account for DOM sorption was calculated as follow:

$$124 \quad S = \frac{(1 - e^{-\alpha_{330} \times Z_{photic}})}{\alpha_{330} \times Z_{photic}} \text{ (S4)}$$

125 The ratio of day-average surface solar intensities  $L(330 \text{ nm})$  measured during solar simulating photodegradation  
126 experiments and the Souffel River were estimated from the Greifensee (Switzerland,  $47^\circ 21' 59'' \text{N}$   $8^\circ 39' 42'' \text{E}$ )  
127 (Leifer, 1988) using the following constant:

$$128 \quad \text{Solar simulator: } L_{sim}(330\text{nm}) = 6.05 \times 10^{-2} \text{ mE cm}^{-2} \text{ day}^{-1}$$

$$129 \quad \text{Souffel River: } L_{river}(330\text{nm}) = 4.34 \times 10^{-2} \text{ mE cm}^{-2} \text{ day}^{-1}$$

130

131 Finally the photodegradation rate in the river ( $k_{phot,river}$ ) was estimated as:

$$132 \quad k_{phot,river} = \frac{k_{phot,sim}}{L_{sim}/L_{river}} \times S \text{ (S5)}$$

133 where  $k_{phot,sim}$  was the photodegradation rate during the solar simulating photodegradation under nitrate  
134 conditions.  $k_{phot,sim}$  under nitrate conditions ( $k_{phot,sim} = (1.3 \pm 0.1) \times 10^{-6} \text{ s}^{-1}$ ) could be considered to be the  
135 maximum photodegradation because no dissipation by dissolved organic matter was taken into account (Drouin  
136 et al., 2021). Hence, photodegradation rates might be slightly overestimated.

### 137 **S1.6 Variation of *S*-metolachlor concentration in topsoil.**

138 During the 2019 campaign, *S*-metolachlor concentrations in topsoil were measured, although the associated  $\delta^{13}\text{C}$   
139 values could not be measured due to matrix effects. Therefore,  $\delta^{13}\text{C}$  was estimated from measured *S*-metolachlor  
140 concentrations in topsoils, as validated in a similar agricultural headwater catchment (Payraudeau et al., 2025).

141 Briefly, *S*-metolachlor biodegradation in topsoil is calculated from a corrected first-order constant ( $k_{dyn}$ )  
142 accounting for the observed topsoil temperature ( $T_{obs}$ ) and moisture ( $\theta_{obs}$ ), as follows in Boesten and Linden  
143 (1991):

$$144 \quad k_{dyn} = k_{Ref} \times f_T \times f_\theta \text{ (S6)}$$

145 where  $f_T$  and  $f_\theta$  are the factors that account for the influence of the topsoil temperature and moisture (w/w). The  
 146 factors for the influence of topsoil temperature follow the Arrhenius laws as follows in Walker (1974):

$$147 \quad f_T = \begin{cases} 0 & \text{if, } T_{\text{obs}} \leq T_{\text{ref}} \\ \frac{T_{\text{obs}} - T_{\text{ref}}}{5} \times e^{\frac{E_a}{R} \times \left( \frac{1}{T_{\text{ref}}} - \frac{1}{T_{\text{obs}}} \right)} & \text{if, } T_{\text{ref}} < T_{\text{obs}} \leq (T_{\text{ref}} + 5) \\ e^{\frac{E_a}{R} \times \left( \frac{1}{T_{\text{ref}}} - \frac{1}{T_{\text{obs}}} \right)} & \text{if, } T_{\text{obs}} > (T_{\text{ref}} + 5) \end{cases} \quad (\text{S7})$$

148 where  $T_{\text{ref}}$  is the reference temperature (293.15 K) in Kelvin,  $E_a$  is the *S*-metolachlor activation energy  
 149 ( $2.391 \times 10^3 \text{ J mol}^{-1}$ ) and  $R$  is the gas constant ( $8.314 \text{ J mol}^{-1} \text{ K}^{-1}$ ) (Jaikaew et al., 2017).

150 The relation to soil moisture follows (Walker, 1974):

$$151 \quad f_\theta = \left( \frac{\theta_{\text{obs}}}{\theta_{\text{ref}}} \right)^{\beta_\theta} \quad (\text{S8})$$

152 where  $\beta_\theta$  is a calibration constant and  $\theta_{\text{ref}}$  the reference water content, which was set at 0.5 and 0.2, respectively.  
 153  $\theta_{\text{obs}}$  and  $T_{\text{obs}}$  for the growing season were obtained for the 0–20 cm topsoil at a 8 km spatial resolution for the  
 154 year 2019 by the national weather service (<https://publitheque.meteo.fr>) computed by a daily soil water budget  
 155 model (Habets et al., 2008).

156 Initial *S*-metolachlor concentrations in topsoil were estimated from application rates reported in the farmer  
 157 surveys. *S*-metolachlor doses were assumed to be present within the top 10 cm of topsoil (Silva et al., 2019). Bulk  
 158 soil density was set at  $1.29 \text{ kg dm}^{-3}$  according to the soilgrid data for the agricultural area within the catchment  
 159 (Hengl et al., 2017).

160 Isotope fractionation was predicted from the *S*-metolachlor biodegradation in topsoil using a Rayleigh equation,

$$161 \quad \ln \left( \frac{\delta^{13}\text{C}(t)+1}{\delta^{13}\text{C}_0+1} \right) = \varepsilon_{\text{bulk},C} \times \ln \left( \frac{P(t)}{P_0} \right) \quad (\text{S9})$$

162 where  $\delta^{13}\text{C}_0$  and  $\delta^{13}\text{C}(t)$  represent the predicted isotope signatures of the carbon at time zero and time  $t$  of  
 163 degradation respectively, while  $P(t)/P_0$  is the fraction of remaining pesticides at time  $t$ .

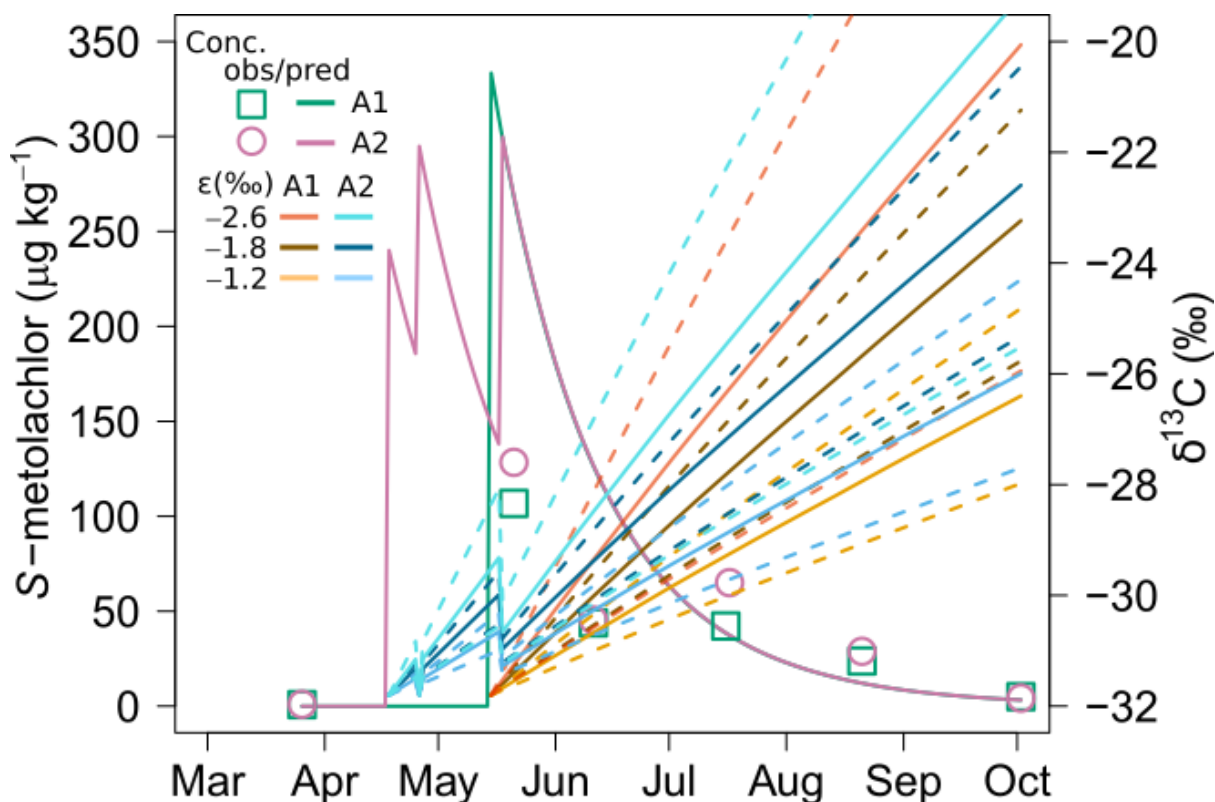
164 Boundary values for biodegradation in soil reported in the literature and defined in this study range from  $\varepsilon_{\text{biodeg},C}$   
 165  $= -2.6 \pm 1.3\text{‰}$  to  $-1.2 \pm 0.4\text{‰}$  (Table S7; (Droz et al., 2021; Torrentó et al., 2021; Alvarez-Zaldívar et al., 2018;  
 166 Meite, 2018). These values were used to determine the extent of degradation. The  $\delta^{13}\text{C}_0$  represents the isotopic  
 167 signature of the commercial product (Table S8) (Alvarez-Zaldívar et al., 2018). The model enables the prediction  
 168 of topsoil *S*-metolachlor concentrations and corresponding  $\delta^{13}\text{C}$  values at a higher temporal resolution than that  
 169 achieved through monthly measurements.

170

171 **Table S7: Range of isotopic enrichment factors for biodegradation ( $\epsilon_{biodeg,C}$ ) of *S*-metolachlor reported in the**  
 172 **literature for various soils and experimental conditions.**

$\epsilon_{biodeg,C}$ (‰)	Soil charact. (% clay/silt/sand organic matter)	Experimental Conditions	References
$-1.50 \pm 0.50$	30.8/61.0/8.5 2.20	aerobic	(Alvarez-Zaldívar et al., 2018)
$-1.20 \pm 0.35$	21.2/67.4/11.4	oxic	(Droz et al., 2021)
$-1.87 \pm 0.58$	17	anoxic	(Droz et al., 2021)
$-1.37 \pm 0.26$	28.3/61.5/10.3	20% water	(Meite, 2018)
$-1.84 \pm 0.26$	1.18	40% water	(Meite, 2018)
$-2.00 \pm 1.20$	11.9/45.1/43.1 1.28	15% water	(Torrentó et al., 2021)
$-2.60 \pm 1.30$	16.0/33.6/50.5 1.72		(Torrentó et al., 2021)
median	$-1.84 \pm 0.50$		

173  
174



175  
176 **Figure S1: Measured and predicted *S*-metolachlor topsoil concentrations at A1 and A2 (Fig. S2). Colored dashed lines**  
 177 **represent the predicted uncertainty of the topsoil  $\delta^{13}C$  calculate using the uncertainty of the isotopic enrichment**  
 178 **factors provided in Table S7.**

179

180 **Table S8: Carbon stable isotope signatures ( $\delta^{13}\text{C}$ ) of commercial products containing *S*-metolachlor.**

Commercial name	$\delta^{13}\text{C}$ (‰)	<i>n</i>
Dual Gold <sup>a</sup>	-31.9 ± 0.2	4
Camix <sup>a</sup>	-31.7 ± 0.2	4
Mercantor Gold <sup>a</sup>	-31.3 ± 0.2	4
Mercantor Gold <sup>b</sup>	-32.2 ± 0.5	3
<i>S</i> -Metolastar <sup>a</sup>	-32.1 ± 0.2	5
<b>average</b>	<b>-31.8 ± 0.3</b>	

181 Uncertainties correspond to the SD from *n* measurements.  
 182 Measured in <sup>a</sup> this study and <sup>b</sup> Alvarez-Zaldívar et al. (2018).  
 183 Samples of the commercial product were provided by the local pesticide supplier  
 184 (Comptoir Agricole) and correspond to the formulation used in the study area.  
 185

### 186 **S1.7 Averaged in-stream transit time and degradation within the river reach between A1 and A2.**

187 Considering no retardation effects in accordance with limited interactions of *S*-metolachlor with the sediment  
 188 riverbed (Lemke et al., 2013), the average in-stream transit time of dissolved *S*-metolachlor within the river reach  
 189 in between A1 and A2 (Fig. S2) is assumed to be similar as the water travel time. A V-shape channel geometry  
 190 of average width 6.5 m and depth 1.5 m ( $m = 6.5/1.5 = 4.3$  the channel bank slope) can be considered as  
 191 representative of the whole river reach. Under uniform and steady state conditions, the normal velocity in the river  
 192 can be estimated with the Manning-Strickler relationship (Akan, 2006) as follow:

$$193 \quad Q_n = K_s \times S \times n \times R_h^{2/3} \times \sqrt{I} \quad (\text{S10})$$

194 where  $Q_n$  refers to the normal velocity in  $\text{m}^3\text{s}^{-1}$ ,  $K_s$  to the Strickler coefficient in  $\text{m}^{1/3}\text{s}^{-1}$  and is equal to  $K_s = 1/n$ ,  
 195  $n$  the Manning's roughness coefficient ( $n$  for clay river beds is 0.030 (Akan, 2006)),  $R_h$  to the hydraulic radius  
 196 in m defined as  $R_h = S/P$  with  $S$  the cross-sectional area in  $\text{m}^2$  and  $P$  the wetted perimeter in m, and  $I$  to the  
 197 average channel slope ( $I = 1.1\%$ ). Under low-flow conditions, with the average water flow rate between A1 and  
 198 A2 ranging from 5 to  $10 \times 10^{-3} \text{ m}^3 \text{ s}^{-1}$ , the normal water height ( $h_n$ ) can be determined to be between 6 and 8 cm  
 199 within the channel, based on the numerical application of Eq. S10. Thus, applying Eq. S11, the average velocity  
 200 ( $v_n$ ) under low flow conditions is estimated between 33 and 40  $\text{cm s}^{-1}$ . Finally, considering the total length of the  
 201 A1–A2 river reach of 2.2 km, under low flow conditions, *S*-metolachlor in-stream transit time within the A1–A2  
 202 river reach is estimated between 1.4 and 1.7 hours.

$$203 \quad Q_n = \frac{v_n}{S} = \frac{v_n}{m \times h_n^2} \quad (\text{S11})$$

### 204 **S1.8 Stable isotope fractionation with increasing *S*-metolachlor in-stream transit time.**

205 Despite the negligible isotope fractionation observed in the sub-catchment A1–A2, CSIA may prove useful for  
 206 larger rivers displaying significantly longer in-stream transit time. Considering no retardation effects in  
 207 accordance with limited interactions of *S*-metolachlor with the sediment riverbed (Lemke et al., 2013), the  
 208 equivalent in-stream transit time ( $t_{eq}$ ) of dissolved *S*-metolachlor within the river reach is considered to be equal  
 209 to the water travel time follow:

210  $t_{eq} = \frac{v_{water}}{L_{water}}$  (S12)

211 where  $v_{water}$  and  $L_{water}$  being the overlying water velocity and the river length respectively. Using laboratory  
 212 derived degradation rates, it is possible to estimate the *S*-metolachlor equivalent in-stream transit time above,  
 213 which can be used with CSIA data to quantify degradation extent instream. The laboratory derived indirect  
 214 photodegradation containing nitrate and dissolved organic matter (Drouin et al., 2021) and oxic biodegradation  
 215 half-lives of *S*-metolachlor are 6 days ( $k_{photo,nitrate+DOM} = (1.3 \pm 0.1) \times 10^{-6} \text{ s}^{-1}$ ) and 29 days ( $k_{biodeg} = (2.7 \pm$   
 216  $0.1) \times 10^{-7} \text{ s}^{-1}$ ), respectively. Contrasted isotopic enrichment factors as been observed for indirect  
 217 photodegradation ( $\varepsilon_{photo,C} = 0.0 \pm 0.0\text{‰}$  in Drouin et al. (2021) and  $-0.4 \pm 0.1\text{‰}$  in Levesque-Vargas et al. (2025))  
 218 and for biodegradation in soil ranging from  $\varepsilon_{biodeg,C} = -2.6 \pm 1.3\text{‰}$  to  $-1.2 \pm 0.4\text{‰}$  (Droz et al., 2021; Torrentó  
 219 et al., 2021; Alvarez-Zaldívar et al., 2018; Meite, 2018). As photodegradation and biodegradation co-occur in  
 220 rivers, the Rayleigh Eq. (S9) was corrected according to Van Breukelen (2007) Eq. (S13):

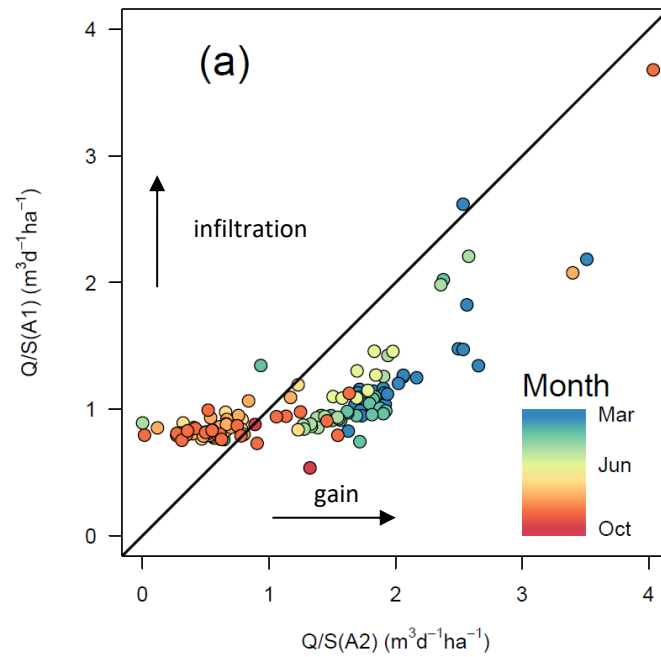
221 
$$\varepsilon_{eff,C} = \frac{k_{photo} \times \varepsilon_{photo,C} + k_{biodeg} \times \varepsilon_{biodeg,C}}{k_{photo} + k_{biodeg,C}} \approx \varepsilon_{biodeg,C}$$
 (S13)

222 with  $\varepsilon_{eff}$  the effective isotopic enrichment factor to be re-injected in Eq. (6) to define the extent of in-stream  
 223 degradation. However, the photodegradation term in Eq. S13 is negligible; consequently, in the present case  
 224 study,  $\varepsilon_{eff,C}$  can be considered equivalent to  $\varepsilon_{biodeg,C}$ . Accordingly, for *S*-metolachlor, isotope fractionation in C  
 225 higher than the threshold of  $\Delta\delta^{13}C_{min} = 2.0 \text{‰}$  is required to reliably confirm the occurrence of *S*-metolachlor  
 226 degradation in rivers with a minimal water in-stream transit time higher than 800 hours.

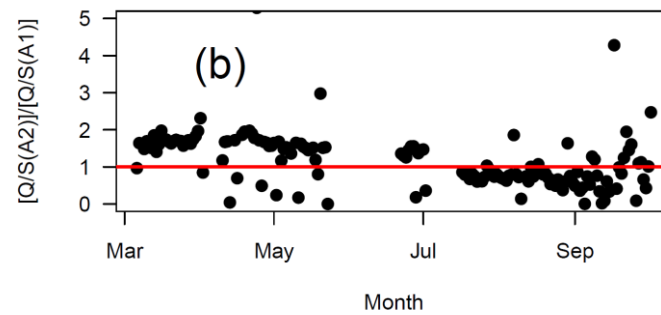
227 However, for longer river reaches the retardation caused by interactions with the riverbed sediment, i.e.,  
 228 contaminant penetration and sorption into the sediment or instream vegetation, may further exacerbate instream  
 229 degradation. Although retardation factors are very case- and molecule-specific a higher-bound value of two may  
 230 be considered for testing the potential of CSIA to quantify instream degradation over long rivers (Liao et al., 2013;  
 231 Salehin et al., 2003). Consequently, a minimal water in-stream transit time of 400 h (17 days) should be achieved  
 232 to measure a significant  $\Delta\delta^{13}C_{min}$ . No equivalent river length was expressed as long equivalent in-stream transit  
 233 times like this one correspond to high Strahler order rivers with flows and velocities varying at each confluence.

234 S2 Supplement results.

235 S2.1 Area-normalized discharges.

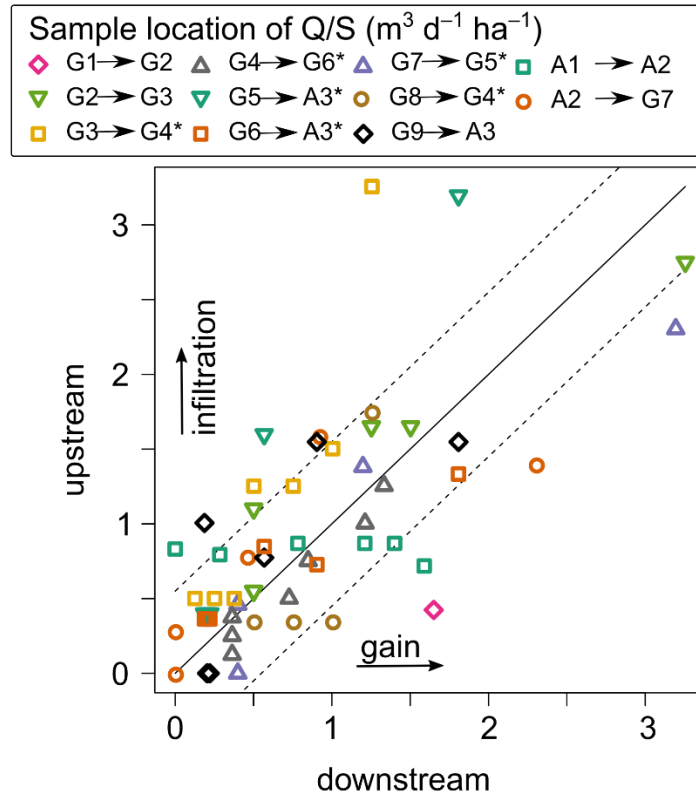


236



237

238 **Figure S2: Area-normalized daily discharges in A1 vs A2. (a) Area-normalized daily discharges of A1 as a function of**  
239 **A2. The black line represents the 1:1 line. Area-normalized daily discharges at the beginning of the monitoring period**  
240 **range from blue to bright yellow. Colors get increasingly red later in the season, indicating a change from strong to**  
241 **light groundwater upwelling fluxes entering the A1–A2 river reach. (b) Area-normalized daily discharge ratios between**  
242 **A1 and A2.**



243

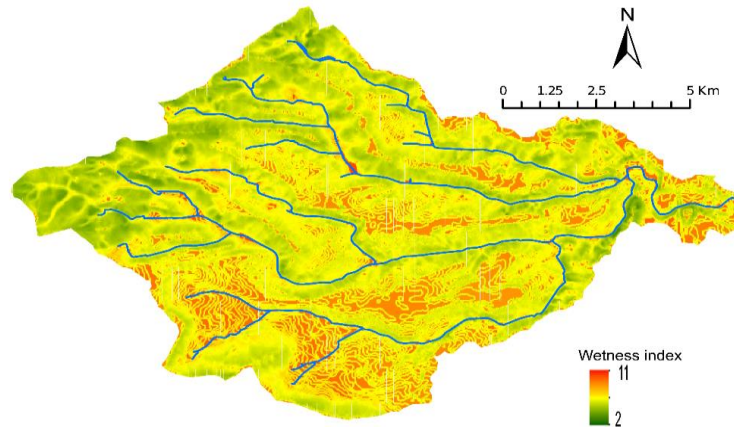
244 **Figure S3: Upstream and downstream normalized flow (Shaw et al., 2019) i.e., discharge divided by surface of the**  
 245 **corresponding sub-catchment, for all grab sampling events. Solid line indicates a 1:1 relationship and dashed line the**  
 246 **95% confidence interval considering a measured flow with 30% uncertainty. Asterisks (\*) highlight reaches with**  
 247 **WWTP contribution.**

## 248 S2.2 Wetness index.

249 Topographical wetness index (TWI) was used to identify contributing areas prone to generate overland flow (Ali  
 250 et al., 2014) and is computed as follows:

$$251 \quad TWI = \ln(a/\tan(b)) \quad (S14)$$

252 where  $a$  is the upslope area draining through a certain point per unit contour length and  $\tan(b)$  is the local slope in  
 253 radians. The catchment has a very low TWI ( $6.5 \pm 1.4$  ( $\bar{x} \pm \text{SD}$ )) with only 7.5% of the riverbank associated with  
 254 a TWI higher than 8.5, which suggests that only a limited area likely contributed to overland runoff (Fig. S4). The  
 255 EU-DEM 2011 was used to calculate TWI using SAGA-GIS 2.3.2+ through RSAGA package v1.3.0.



256

257 **Figure S4: Topographical wetness index (TWI) of the Souffel catchment.**

258 **S2.3 S-metolachlor concentrations per location.**

259 **Table S9: S-metolachlor average concentrations ( $\bar{x}$ ), standard deviation (SD), minimal and maximal concentration**  
 260 **(min–max), frequency of the detection (freq.) and number of samples investigated (n) per location during the sampling**  
 261 **period.**

	dissolved				particulate				sediment			
	S-metolachlor ( $\mu\text{g L}^{-1}$ )				S-metolachlor ( $\mu\text{g kg}^{-1}$ )				S-metolachlor ( $\mu\text{g kg}^{-1}$ )			
	$\bar{x} \pm \text{SD}$ (min–max)	freq. (%)	n.		$\bar{x} \pm \text{SD}$ (min–max)	freq. (%)	n.	$\bar{x} \pm \text{SD}$ (min–max)	freq. (%)	n.		
<b>continuous samples at the outlet</b>												
A1	0.74 $\pm$ 2.22	(0.02–14.3)	86	58	< LD	0	9	6.79 $\pm$ 7.18	(1.72–11.9)	29	7	
A2	0.48 $\pm$ 0.80	(0.02–5.37)	96	69	< LD	0	24	2.47	(2.46)	13	8	
A3	2.24 $\pm$ 7.11	(0.03–54.6)	96	67	< LD	0	35	3.48	(3.48)	17	6	
<b>A1–3</b>	<b>1.18 <math>\pm</math> 4.47</b>	<b>(0.02–54.6)</b>	<b>93</b>	<b>194</b>	<b>&lt; LD</b>	<b>0</b>	<b>68</b>	<b>4.88 <math>\pm</math> 4.71</b>	<b>(1.72–11.9)</b>	<b>19</b>	<b>21</b>	
<b>grab samples</b>												
G1	0.14 $\pm$ 0.25	(0.02–0.59)	71	7	< LD	0	2	< LD		0	1	
G2	3.69 $\pm$ 8.71	(0.02–21.5)	86	7	< LD	0	2	< LD		0	7	
G3	0.32 $\pm$ 0.42	(0.06–0.94)	57	7	< LD	0	1	< LD		0	7	
G4	0.99 $\pm$ 1.15	(0.14–2.66)	57	7	< LD	0	4	< LD		0	7	
G5	0.26 $\pm$ 0.16	(0.10–0.51)	71	7	< LD	0	1	7.38 $\pm$ 3.01	(5.26–9.51)	29	7	
G6	0.82 $\pm$ 1.12	(0.03–2.73)	71	7	< LD	0	4	5.15	(5.15)	14	7	
G7	0.09 $\pm$ 0.04	(0.02–0.13)	71	7	n.m.			< LD		0	7	
G8	0.17 $\pm$ 0.21	(0.03–0.41)	75	4	< LD	0	1	< LD		0	5	
G9	0.98 $\pm$ 1.78	(0.09–4.16)	71	7	< LD	0	3	6.09	(6.09)	14	7	
<b>G1–9</b>	<b>0.94 <math>\pm</math> 3.35</b>	<b>(0.02–21.5)</b>	<b>72</b>	<b>60</b>	<b>&lt; LD</b>	<b>0</b>	<b>18</b>	<b>6.5 <math>\pm</math> 2.0</b>	<b>(5.15–9.51)</b>	<b>7</b>	<b>55</b>	
<b>all river samples</b>												
<b>A1–G9</b>	<b>1.13 <math>\pm</math> 4.28</b>	<b>(0.02–54.6)</b>	<b>88</b>	<b>254</b>		<b>0</b>	<b>86</b>	<b>5.69 <math>\pm</math> 3.47</b>	<b>(1.72–11.9)</b>	<b>11</b>	<b>76</b>	
<b>grab wastewater treatment plant (WWTPs) samples</b>												
W1	0.40 $\pm$ 0.54	(0.01–1.28)	100	7	n.m.			n.m.				
W2	0.30 $\pm$ 0.32	(0.01–0.96)	100	7	< LD	0	2	n.m.				
W3	8.9 $\pm$ 20.2	(0.26–50.2)	86	7	< LD	0	2	n.m.				
<b>W1–3</b>	<b>2.9 <math>\pm</math> 11.1</b>	<b>(0.01–50.2)</b>	<b>95</b>	<b>21</b>	<b>&lt; LD</b>	<b>0</b>	<b>4</b>	<b>n.m.</b>				
<b>soil samples</b>												
<b>S-metolachlor (<math>\mu\text{g kg}^{-1}</math>)</b>												
	$\bar{x} \pm \text{SD}$ (min–max)		freq. (%)	n.								
A1	37.1 $\pm$ 38.6		(0.82–107)	100	6							
A2	45.5 $\pm$ 47.4		(0.99–128)	100	6							

262

263 n.m. not measured, < LD below limit of detection which is 1.2  $\mu\text{g kg}^{-1}$ .

264 **S2.4 Detailed off-site transport of *S*-metolachlor per event**

265 Over 9% of the seasonal *S*-metolachlor exports (Events 1 and 2; Table S10) occurred before the first recorded  
 266 applications. This early export cannot be fully explained by residual topsoil *S*-metolachlor from the previous year,  
 267 which the mass balance (Table S11) estimated to contribute only 0.8–1.5% of the seasonal load. Events 8 and 12  
 268 triggered sharp increases in *S*-metolachlor concentrations, reaching approximately 5 µg L<sup>-1</sup> at sites A1 and A2.  
 269 These events accounted for 17.5% and 29.5% of the total exports at A1 and A2, respectively. Although runoff  
 270 was considered unlikely during Event 12, its cumulative rainfall (36 mm)—the highest of the season—may have  
 271 induced localized surface runoff.

272

273 Subsurface flow during moderate rainfall events (excluding Events 8 and 15) also contributed significantly,  
 274 representing 28.5% and 70.5% of the total load at A1 and A2, respectively. While intense rainfall events caused  
 275 the largest individual exports, subsurface transport played a dominant role over time. A single rainfall event on  
 276 May 18, just two days after *S*-metolachlor application on corn, was responsible for 54% of the total seasonal  
 277 export at A1, with a peak concentration of 14.33 µg L<sup>-1</sup>. This export likely occurred via lateral subsurface flow,  
 278 consistent with transport patterns during other moderate post-application rainfall events (10–16 mm h<sup>-1</sup>) (Lefrancq  
 279 et al., 2017). Flash export in clayey soils by preferential flows in soil cracks may also explain the transient  
 280 character of this event, as described for bentazone and MCPA (2-methyl-4-chlorophenoxyacetic acid) and other  
 281 pesticides (Kronvang et al., 2004).

282

283 **Table S10: *S*-metolachlor concentrations and load dynamics at the outlet of the Souffel catchment for the main rainfall**  
 284 **events (export of 91% of the seasonal load).**

Event	1+2	3 <sup>b</sup>	4	5	6 <sup>b</sup>	7
Duration (hours) <sup>a</sup>	99 ± 24	101	80 ± 4	7 ± 6	1	42 ± 53
Amount (mm) <sup>a</sup>	28 ± 14	11	26 ± 9	11 ± 8	2.6	18 ± 14
Days since last application (d)	p.a.	8 <sup>c</sup>	20 <sup>d</sup>	15 <sup>e</sup>	17 <sup>e</sup>	21 <sup>e</sup>
Mass applied (kg) <sup>f</sup>	0 (%)	160 ± 6 (5%)	319 ± 12 (10%)		3163 ± 116 (100%)	
Max con. (µg L <sup>-1</sup> )	2.56	1.51	1.45	6.28	0.07	3.10
Load (kg) <sup>g</sup>	0.44 (9%)	0.57 (12%)	0.44 (9%)	2.28 (47%)	0.44 (9%)	0.29 (5%)
Max flow (m <sup>3</sup> s <sup>-1</sup> )	0.85	0.28	0.61	2.20	0.14	0.61

285 <sup>a</sup> considers rainfall gages R1, R2 and R9 only, <sup>b</sup> rainfall event detected only in R1, <sup>c, d, e</sup> considers application dates  
 286 of April 18, April 29 and May 20, 2019, respectively, according to the survey of sub-catchment A2 (Section S1.1).  
 287 <sup>f</sup> accounts for the realistic scenario (Table S1), percent of the total mass applied in parentheses, <sup>g</sup> loads  
 288 corresponding to the rainfall event, percent of the total load in parentheses. p.a. pre-application. Average flow  
 289 discharge is 0.115 m<sup>3</sup> s<sup>-1</sup>.

290

291

292 **S2.5 Pesticide mass balance**

293 A seasonal mass balance of *S*-metolachlor at the catchment scale—from application through October—was  
294 established using data from laboratory experiments, field observations, and river monitoring (Eq. 3; Table S11).  
295 At the field scale, volatilization was modeled based on soils, climate, and crop types comparable to those in the  
296 study area (Table S6), suggesting that 2.2–5.5% of the applied *S*-metolachlor volatilized within one day of  
297 application. Prior to this study, off-site transport of *S*-metolachlor from agricultural topsoil to surface and  
298 groundwater at the catchment scale was poorly quantified. Monitoring results showed that this transport accounted  
299 for less than 1% of the applied mass in the upstream reach (A1–A2), and less than 0.1% at the full catchment scale  
300 in 2019.

301  
302 Due to short water residence times, in-river biodegradation was limited, with an estimated contribution of  
303  $2.7 \pm 2.3\%$  (average  $\pm$  SD). Additional degradation processes included 0.3% at the sediment–water interface under  
304 anoxic conditions and 10% via photolysis in the water column, both estimated using first-order kinetics and  
305 representing point and non-point sources. The *S*-metolachlor load measured at the catchment outlet represented  
306 only 0.05–0.1% of the total applied amount. The mass balance closed within a 2% margin of error and indicated  
307 that  $98.9 \pm 4.7\%$  of the applied *S*-metolachlor was degraded during the season, accounting for uncertainties in  
308 application scenarios.

309  
310 This balance, supported by monthly concentration data from topsoil, river water, and WWTP effluents, and by  
311 continuous load monitoring at the outlet, was compared with degradation estimates from monthly CSIA  
312 measurements. As *S*-metolachlor does not exhibit isotope fractionation under photolysis, CSIA results reflect  
313 biodegradation exclusively (Drouin et al., 2021). In October, biodegradation estimates derived from CSIA and  
314 mass balance were in strong agreement, yielding values of  $98 \pm 20\%$  and  $98.9 \pm 4.7\%$  (average  $\pm$  SD),  
315 respectively. While CSIA exhibited higher analytical uncertainty, its advantages include minimal data  
316 requirements, contrasting with the extensive sampling and multiple assumptions required to establish a catchment-  
317 scale mass balance.

318

319 **Table S11: Mass balance at the catchment scale A3 in the agricultural field and river.**

	Unit	$\bar{x} \pm SD$ (min–max)
Catchment area	km <sup>2</sup>	120
Application area <sup>a</sup>	km <sup>2</sup>	64.5 ± 2.2
<i>S-metolachlor application and stock in the soil</i>		
Stock in the soil (top 10 cm) before applications <sup>b</sup>	kg	7.49 ± 0.26
Maximal scenario	kg	8919
Economic scenario	kg	5969
Realistic scenario (survey)	kg	3163 ± 116
Stock in the soil (top 10 cm) after 214 days <sup>b</sup>	kg	38.2 ± 1.3
<i>Hydrology<sup>c</sup></i>		
Outflow discharge (0–214 days)	m <sup>3</sup> day <sup>-1</sup>	8800 ± 9050 (1400–72,270)
<i>Erosion<sup>c</sup></i>		
TSS export (0–214 Days)	t	720
<i>S-metolachlor export in runoff/discharge<sup>c</sup></i>		
Dissolved export (0–214 days)	kg	4.87 ± 1.00
Particulate export (0–214 days)	kg	n.o.
Total export (dissolve and particulate) (0–214 days) <sup>d</sup>	%	(0.04 – 0.19)
WWTP S-metolachlor load <sup>e</sup>	%	49 ± 6
	kg	2.4 ± 0.8
<i>Dissipation process in the river stretch</i>		
Sorption in sediment bed		n.o.
Hydrolysis (0–214 days)		n.o.
Hyporheic exchange		n.m.
Photolysis (0–214 days)	%	10.4 ± 2.9
	g	506 ± 23
River biodegradation (0–214 days)	%	2.7 ± 2.3
	g	131 ± 20
<i>Dissipation process at the catchment</i>		
Volatilization (0–36 h after application)	%	(2.2 – 5.5)
<b>Total biodegradation (0–214 days)</b>	<b>%</b>	<b>98.9 ± 4.7</b>
<b>(account for all degradation process)</b>	<b>kg</b>	<b>(4740 – 9337)</b>
Remaining mass unaccounted for <sup>d</sup>	kg	(91 – 142)
	%	1.50 – 1.90

320 <sup>a</sup> calculated based on Table S1. <sup>b</sup> extrapolated from the topsoil data in the vicinity of A1 and A2 (n = 2). <sup>c</sup> data  
321 from the outlet of the catchment (n = 67), <sup>d</sup> range covered by the three scenarios. <sup>e</sup> estimated from grab sampling  
322 (n= 7 x 3 locations). n.o. not occurring, n.m. not measured.  
323

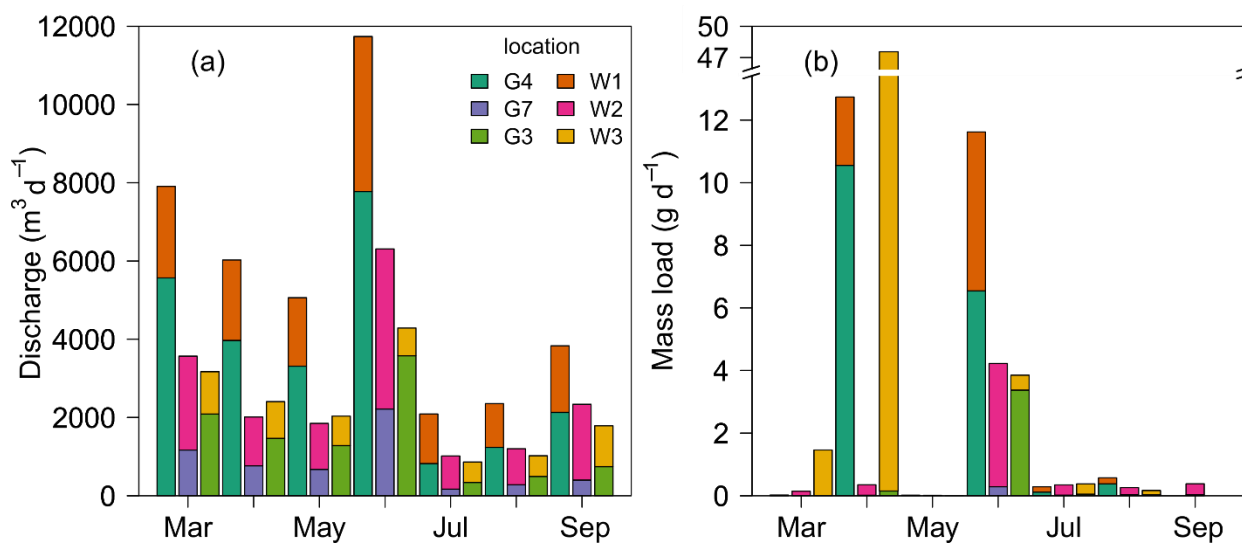
## S2.6 Hydrochemistry

325 Significant differences were observed between river (A1-3 and G1-9) and WWTP (W1-3) outlet samples, with higher chloride, sodium and potassium concentrations observed in the WWTP outlets (Tukey's test;  $p < 0.01$ ). Conversely, nitrate concentrations in the river ( $\bar{x} \pm SD = 41.2 \pm 18.4 \text{ mg L}^{-1}$ ;  $n = 84$ ; Table S12) were higher than those at the WWTP outlets ( $p < 0.01$ ;  $\bar{x} \pm SD = 16.2 \pm 18.0 \text{ mg L}^{-1}$ ;  $n = 21$ ; Table S12). This indicates that a significantly larger proportion of nitrate comes from non-point sources versus WWTP effluent.

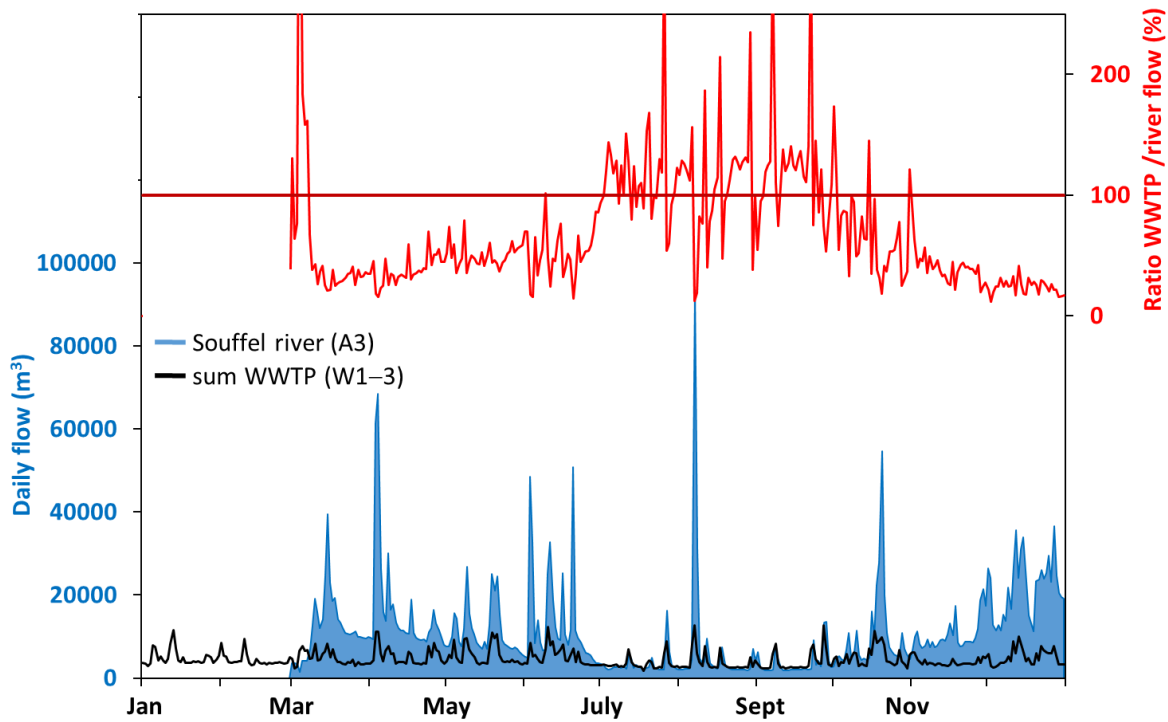
330 **Table S12: Water composition during grab sampling at each location ( $\bar{x} \pm SD$ ;  $n = 7$  per location).**

loc.	pH (-)	cond. (mS cm <sup>-1</sup> )	T (°C)	TSS (mg L <sup>-1</sup> )	DOC (mg L <sup>-1</sup> )	NH <sub>4</sub> <sup>+</sup> (mg L <sup>-1</sup> )	Na <sup>+</sup> (mg L <sup>-1</sup> )	K <sup>+</sup> (mg L <sup>-1</sup> )	Mg <sup>2+</sup> (mg L <sup>-1</sup> )	Ca <sup>2+</sup> (mg L <sup>-1</sup> )	Cl <sup>-</sup> (mg L <sup>-1</sup> )	NO <sub>3</sub> <sup>-</sup> (mg L <sup>-1</sup> )	SO <sub>4</sub> <sup>2-</sup> (mg L <sup>-1</sup> )	HCO <sub>3</sub> <sup>-</sup> (mg L <sup>-1</sup> )	CO <sub>3</sub> <sup>2-</sup> (mg L <sup>-1</sup> )
G1	9.0 ± 0.7	0.931 ± 0.023	14.2 ± 2.2	105 ± 102	1.54 ± 0.48	0.00 ± 0.00	6.8 ± 0.4	2.4 ± 0.3	56 ± 2	130 ± 14	26 ± 2	56 ± 2	169 ± 18	301 ± 114	53 ± 45
G2	8.5 ± 1.1	1.190 ± 0.122	16.4 ± 3.2	82 ± 112	1.87 ± 0.54	0.08 ± 0.16	10.5 ± 1.4	4.9 ± 0.6	41 ± 5	185 ± 24	31 ± 4	41 ± 5	364 ± 58	326 ± 103	41 ± 62
G3	8.9 ± 0.8	1.057 ± 0.301	16.5 ± 3.1	181 ± 197	3.58 ± 1.92	0.34 ± 0.77	25.6 ± 34.5	8.0 ± 7.3	34 ± 16	143 ± 53	51 ± 30	34 ± 16	231 ± 116	320 ± 92	71 ± 90
G4	8.1 ± 0.5	1.165 ± 0.104	13.3 ± 3.9	580 ± 708	5.83 ± 5.26	10.35 ± 7.37	29.1 ± 9.9	8.7 ± 2.0	26 ± 7	158 ± 9	53 ± 6	26 ± 7	234 ± 47	382 ± 117	57 ± 122
G5	8.2 ± 0.5	0.900 ± 0.162	14.1 ± 3.4	136 ± 93	4.91 ± 1.14	0.38 ± 0.49	54.2 ± 22.9	12.3 ± 4.5	37 ± 13	111 ± 29	89 ± 33	37 ± 13	75 ± 11	383 ± 109	11 ± 14
G6	7.8 ± 0.4	1.061 ± 0.157	13.0 ± 3.9	784 ± 976	6.97 ± 6.62	7.77 ± 5.57	43.9 ± 16.8	11.8 ± 3.8	24 ± 9	132 ± 16	71 ± 20	24 ± 9	181 ± 29	397 ± 85	4 ± 5
G7	8.3 ± 0.5	0.837 ± 0.339	14.7 ± 2.8	108 ± 167	2.87 ± 0.53	0.67 ± 1.26	20.0 ± 4.9	4.1 ± 1.5	52 ± 11	140 ± 18	61 ± 7	52 ± 11	81 ± 9	443 ± 72	19 ± 27
G8	8.5 ± 0.3	0.831 ± 0.044	15.0 ± 3.9	149 ± 222	3.62 ± 0.55	0.53 ± 0.98	27.0 ± 3.4	8.1 ± 3.3	31 ± 4	114 ± 18	66 ± 8	31 ± 4	77 ± 10	371 ± 65	16 ± 10
G9	8.4 ± 0.4	1.076 ± 0.066	14.2 ± 3.6	57 ± 51	5.25 ± 4.96	0.19 ± 0.34	36.1 ± 40.2	8.2 ± 5.2	35 ± 15	158 ± 46	78 ± 52	35 ± 15	179 ± 66	396 ± 93	14 ± 19
G10	8.8 ± 0.8	1.056 ± 0.141	15.4 ± 0.9	20 ± 15	2.23 ± 0.93	0.87 ± 2.05	12.1 ± 1.1	4.6 ± 1.5	70 ± 14	158 ± 27	33 ± 4	70 ± 14	187 ± 40	345 ± 116	62 ± 67
G11	8.9 ± 0.8	0.943 ± 0.261	15.0 ± 1.5	273 ± 551	3.84 ± 2.12	0.23 ± 0.50	10.8 ± 2.6	3.8 ± 0.8	65 ± 17	143 ± 45	37 ± 12	65 ± 17	147 ± 56	305 ± 113	65 ± 70
W1	7.4 ± 0.4	0.937 ± 0.208	16.8 ± 4.1	11 ± 6	8.32 ± 5.92	0.60 ± 0.79	96.8 ± 25.8	19.3 ± 4.5	13 ± 12	58 ± 14	134 ± 36	13 ± 12	65 ± 15	267 ± 81	3 ± 7
W2	7.7 ± 0.6	0.923 ± 0.197	17.1 ± 4.6	81 ± 140	8.10 ± 2.99	8.86 ± 20.74	84.9 ± 21.7	22.6 ± 6.1	22 ± 21	69 ± 14	104 ± 24	22 ± 21	72 ± 12	311 ± 85	43 ± 109
W3	8.3 ± 1.2	1.169 ± 0.201	17.1 ± 4.4	184 ± 263	6.36 ± 3.51	26.23 ± 20.13	58.6 ± 36.1	13.6 ± 6.2	14 ± 21	108 ± 65	76 ± 28	14 ± 21	150 ± 136	429 ± 157	24 ± 35
A	7.4 ± 0.3	0.967 ± 0.175	14.5 ± 2.2	488 ± 473	5.19 ± 1.84	4.36 ± 2.53	47.8 ± 19.1	11.8 ± 3.6	25 ± 13	110 ± 23	75 ± 24	25 ± 13	131 ± 30	351 ± 99	1 ± 1

## S2.7 Wastewater treatment plant (WWTP) contribution



335 Figure S5: Contribution of river and WWTPs to the total reach discharge (a) and associated *S*-metolachlor loads (b) for monthly sampling. G4, G7 and G3 were located directly upstream of the effluents of WWTPs 1, 2 and 3, respectively. Note that G4 is downstream of G3, and W3 thus contributed to the G4 discharge.



340 **Figure S6: Daily flow in 2019 at the catchment outlet (A3) and sum of the wastewater treatment plant (WWTP) outflow. Ratio between the two flows higher than 100% indicates when the flow at A3 was lower than the sum of WWTP flow, indicating uptake by riparian vegetation and infiltration from the river into groundwater through the hyporheic**

## S2.8 S-metolachlor transformation products

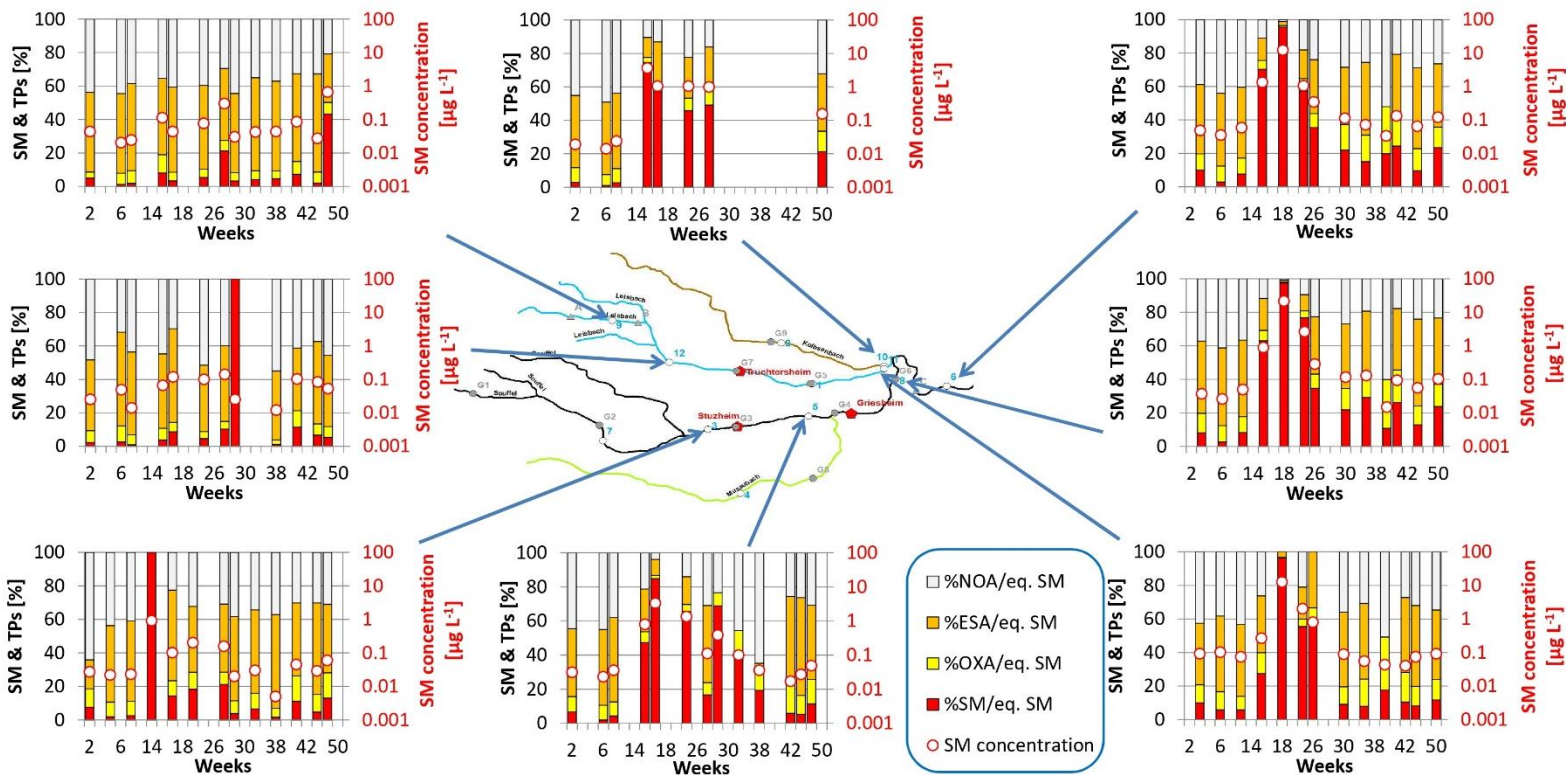
**Table S13: Contributions of three S-metolachlor (SM) transformation products (TPs = metolachlor ethane sulfonic acid (ESA), metolachlor oxanilic acid (OXA) and metolachlor NOA 413173) to the total concentration of S-metolachlor and its transformation products (MEL<sub>SM</sub>, expressed as molar equivalents of S-metolachlor) across eight monthly monitoring stations of the Rhin-Meuse Water Agency in 2019. Data are presented as average ± standard deviation per month, per season (Spring: A-M-J; Summer: J-A-S; Fall: O-N-D and winter: J-F-M) and for the 2019 year (Dataset available on <https://naiades.eaufrance.fr/donnees-disponibles>).**

Month (2019)	%SM/MEL <sub>SM</sub>	%TPs/MEL <sub>SM</sub>	%ESA/MEL <sub>SM</sub> *	%OXA/MEL <sub>SM</sub> *	%SM/MEL <sub>SM</sub> *	(%ESA + %OXA) / %TPs
January (n= 8)	6.6 ± 3.0%	93.4 ± 3.0%	70.7 ± 11.8%	17.0 ± 6.7%	12.3 ± 6%	51.2 ± 8.8%
February (n = 8)	2.5 ± 1.5%	97.5 ± 1.5%	80.6 ± 4.2%	15.2 ± 2.0%	4.3 ± 2.4%	56.8 ± 5.0%
March (n = 8)	4.3 ± 2.8%	95.7 ± 2.8%	79.1 ± 5.9%	13.8 ± 1.6%	7.1 ± 4.5%	57.6 ± 2.6%
April (n = 7)	42.1 ± 29.4%	57.9 ± 29.4%	39.9 ± 27.0%	10.2 ± 5.4%	50 ± 31.6%	61.3 ± 4.6%
May (n = 11)	56.2 ± 34.9%	43.8 ± 34.9%	30.5 ± 30.3%	6.2 ± 4.6%	63.3 ± 33.7%	62.8 ± 13.9%
June (n = 8)	30.9 ± 16.6%	69.1 ± 16.6%	51.0 ± 16.7%	10.1 ± 2.1%	38.8 ± 15.6%	67.3 ± 13.7%
July (n = 6)	21.4 ± 24.7%	78.6 ± 24.7%	56.1 ± 31.3%	14.5 ± 4.8%	29.4 ± 31.6%	54.8 ± 15.1%
August (n = 3)	16.0 ± 18.5%	84.0 ± 18.5%	53.8 ± 46.9%	17.9 ± 12.1%	28.3 ± 34.9%	51.4 ± 20.8%
September (n = 7)	10.7 ± 8.4%	89.3 ± 8.4%	38.0 ± 47.4%	37.5 ± 29.5%	24.5 ± 20.9%	42.0 ± 15.5%
October (n = 7)	13.8 ± 8.1%	86.2 ± 8.1%	60.7 ± 10.8%	20.6 ± 5.3%	18.7 ± 9.4%	67.9 ± 7.5%
November (n = 7)	7.1 ± 3.6%	92.9 ± 3.6%	75.6 ± 7.0%	14.4 ± 3.2%	10 ± 4.7%	67.6 ± 4.3%
December (n = 7)	19.2 ± 11.8%	80.8 ± 11.8%	56.8 ± 12.3%	16.7 ± 4.4%	26.5 ± 14%	62.5 ± 5.3%
Spring (n = 26)	44.6 ± 29.9%	55.4 ± 29.9%	39.3 ± 26.4%	8.5 ± 4.5%	52.2 ± 29.6%	63.8 ± 11.9%
Summer (n = 16)	15.7 ± 17.4%	84.3 ± 17.4%	47.8 ± 40.0%	25.2 ± 22.4%	27 ± 26%	48.5 ± 16.3%
Fall (n = 22)	13.6 ± 9.7%	86.4 ± 9.7%	64.0 ± 12.9%	17.2 ± 4.9%	18.8 ± 12.1%	65.8 ± 6.1%
Winter (n = 24)	4.4 ± 2.9%	95.6 ± 2.9%	76.8 ± 8.8%	15.3 ± 4.2%	7.9 ± 5.5%	55.2 ± 6.5%
Year (n = 88)	20.7 ± 24.4%	79.3 ± 24.4%	57.2 ± 27.7%	15.6 ± 11.7%	27.2 ± 26.8%	59.2 ± 12.2%

MEL<sub>SM</sub> is calculated with equation S1 with ESA, OXA and NOA, and only with ESA and OXA for MEL<sub>SM</sub>\* to be comparable to Rose et al. (2018).

$$MEL_{SM} = load(SM) + \sum_{i=1}^{TPs} load(TP_i) \times \frac{MW_{SM}}{MW_{TP_i}} \quad (S1)$$

where  $MW_{SM}$  and  $MW_{TP_i}$  correspond to the molar weight of S-metolachlor, and that of its TPs, respectively. The proportion of each TPs, i.e. %ESA, %OXA and %NOA, can be expressed as the ratio of the associated mass equivalent loads on the MEL<sub>SM</sub> or the MEL<sub>SM</sub>\*.



355 **Figure S7:** *S*-metolachlor (SM) concentrations at the eight monthly monitoring stations of the Rhin-Meuse Water Agency in 2019 are presented on a logarithmic scale ( $0.001$  to  $100 \mu\text{g L}^{-1}$ ) using the secondary y-axis on the right side of each graph. These concentrations are depicted as red circles with white fill. The relative contributions of three transformation products (TPs) - metolachlor ethane sulfonic acid (ESA), metolachlor oxanilic acid (OXA), and metolachlor NOA 413173 - to the total concentration (*S*-metolachlor plus transformation products, expressed in molar equivalents of *S*-metolachlor) are shown on the secondary y-axis on the left side of each graph.

360

**Table S14: Analytical method description for the transformation products of *S*-metolachlor (ISO/IEC 17025-accredited laboratory - Eurofins Hydrologie Est, NF EN ISO 11369).**

365

Parameters	Quantification limit (µg/L)	Uncertainty method	Extraction method*	Separation method	Detection method	Analytical method
<i>S</i> -metolachlor ESA	0.01		SPE			
<i>S</i> -metolachlor OXA	0.005	NF ISO 11352	SPE	HPLC	MS/MS	Modified NF ISO 11369
<i>S</i> -metolachlor NOA 413173	0.02		SPE			
<i>S</i> -metolachlor	0.005		LLE			

\* SPE: Solid-Phase Extraction; LLE: Liquid-Liquid Extraction

370

### S3 Supplement references

- Akan, A. O.: 3-Normal flow, in: Open Channel Hydraulics, edited by: Akan, A. O., Butterworth-Heinemann, Oxford, 67–96, 2006.
- 375 Ali, G., Birkel, C., Tetzlaff, D., Soulsby, C., McDonnell, J. J., and Tarolli, P.: A comparison of wetness indices for the prediction of observed connected saturated areas under contrasting conditions, *Earth Surf. Proc. Land.*, 39, 399–413, <https://doi.org/10.1002/esp.3506>, 2014.
- Alvarez-Zaldívar, P., Payraudeau, S., Meite, F., Masbou, J., and Imfeld, G.: Pesticide degradation and export losses at the catchment scale: Insights from compound-specific isotope analysis (CSIA), *Water Res.*, 139, 198–207, <https://doi.org/10.1016/j.watres.2018.03.061>, 2018.
- 380 Bauer-Marschallinger, B., Paulik, C., Hochstoger, S., Mistelbauer, T., Modanesi, S., Ciabatta, L., Massari, C., Brocca, L., and Wagner, W.: Soil moisture from fusion of scatterometer and SAR: Closing the scale gap with temporal filtering, *Remote Sensing*, 10, 1030, <https://doi.org/10.3390/rs10071030>, 2018.
- Boesten, J. and Linden, A.: Modeling the influence of sorption and transformation on pesticide leaching and persistence, *Journal of Environment Quality*, 20, 425–435, <https://doi.org/10.2134/jeq1991.00472425002000020015x>, 1991.
- 385 Davie-Martin, C. L., Hageman, K. J., and Chin, Y.-P.: An improved screening tool for predicting volatilization of pesticides applied to soils, *Environ. Sci. Technol.*, 47, 868–876, <https://doi.org/10.1021/es3020277>, 2013.
- Drouin, G., Droz, B., Leresche, F., Payraudeau, S., Masbou, J., and Imfeld, G.: Direct and indirect photodegradation of atrazine and *S*-metolachlor in agriculturally impacted surface water and associated C and N isotope fractionation, *Environ. Sci. Process. Impacts*, 23, 1791–1802, <https://doi.org/10.1039/D1EM00246E>, 2021.
- 390 Droz, B., Drouin, G., Lohmann, J., Guyot, B., Payraudeau, S., and Imfeld, G.: Data for "How combining multi-scale monitoring and compound-specific isotope analysis helps to evaluate degradation of the herbicide *S*-metolachlor in agro-ecosystems?" (v1.0), Zenodo [dataset], <https://doi.org/10.5281/zenodo.6414880>, 2025.
- Droz, B., Drouin, G., Maurer, L., Villette, C., Payraudeau, S., and Imfeld, G.: Phase transfer and biodegradation of pesticides in water-sediment systems explored by compound-specific isotope analysis and conceptual modeling, *Environ. Sci. Technol.*, 55, 4720–4728, <https://doi.org/10.1021/acs.est.0c06283>, 2021.
- 395 Fono, L. J., Kolodziej, E. P., and Sedlak, D. L.: Attenuation of wastewater-derived contaminants in an effluent-dominated river, *Environ. Sci. Technol.*, 40, 7257–7262, <https://doi.org/10.1021/es061308e>, 2006.
- Gish, T. J., Prueger, J. H., Daughtry, C. S. T., Kustas, W. P., McKee, L. G., Russ, A. L., and Hatfield, J. L.: Comparison of field-scale herbicide runoff and volatilization losses: An eight-year field investigation, *J. Environ. Qual.*, 40, 1432–1442, <https://doi.org/10.2134/jeq2010.0092>, 2011.
- 400 Habets, F., Boone, A., Champeaux, J. L., Etchevers, P., Franchistéguy, L., Leblois, E., Ledoux, E., Le Moigne, P., Martin, E., Morel, S., Noilhan, J., Quintana Seguí, P., Rousset-Regimbeau, F., and Viennot, P.: The SAFRAN-ISBA-MODCOU hydrometeorological model applied over France, *Journal of Geophysical Research: Atmospheres*, 113, D06113, <https://doi.org/10.1029/2007jd008548>, 2008.
- 405 Hengl, T., Mendes de Jesus, J., Heuvelink, G. B. M., Ruiperez Gonzalez, M., Kilibarda, M., Blagotić, A., Shangguan, W., Wright, M. N., Geng, X., Bauer-Marschallinger, B., Guevara, M. A., Vargas, R., MacMillan, R. A., Batjes, N. H., Leenaars, J. G. B., Ribeiro, E., Wheeler, I., Mantel, S., and Kempen, B.: SoilGrids250m: Global gridded soil information based on machine learning, *PLoS One*, 12, e0169748, <https://doi.org/10.1371/journal.pone.0169748>, 2017.

- Hippelein, M. and McLachlan, M. S.: Soil/air partitioning of semivolatile organic compounds. 2. Influence of temperature and relative humidity, *Environ. Sci. Technol.*, 34, 3521–3526, <https://doi.org/10.1021/es991421n>, 2000.
- 410 Huang, L. Q. and Frink, C. R.: Distribution of atrazine, simazine, alachlor, and metolachlor in soil profiles in Connecticut, *Bull. Environ. Contam. Toxicol.*, 43, 159–164, <https://doi.org/10.1007/BF01702253>, 1989.
- Jaikaew, P., Malhat, F., Boulange, J., and Watanabe, H.: Aspect of the degradation and adsorption kinetics of atrazine and metolachlor in andisol soil, *Hellenic Plant Protection Journal*, 10, 1–14, <https://doi.org/10.1515/hppj-2017-0001>, 2017.
- Kronvang, B., Strøm, H., Hoffmann, C. C., Laubel, A., and Friberg, N.: Subsurface tile drainage loss of modern pesticides: field experiment results, *Water Sci. Technol.*, 49, 139–147, <https://doi.org/10.2166/wst.2004.0181>, 2004.
- 415 Lefrancq, M., Van Dijk, P., Jetten, V., Schwob, M., and Payraudeau, S.: Improving runoff prediction using agronomical information in a cropped, loess covered catchment, *Hydrol. Process.*, 31, 1408–1423, <https://doi.org/10.1002/hyp.11115>, 2017.
- Leifer, A.: *The kinetics of environmental aquatic photochemistry: Theory and practice*, American Chemical Society, 336 pp.1988.
- Lemke, D., Liao, Z., Wöhling, T., Osenbrück, K., and Cirpka, O. A.: Concurrent conservative and reactive tracer tests in a stream undergoing hyporheic exchange, *Water Resour. Res.*, 49, 3024–3037, <https://doi.org/10.1002/wrcr.20277>, 2013.
- 420 Levesque-Vargas, M., Ohlund, L., Sleno, L., Gelinias, Y., Hohener, P., and Ponsin, V.: Insights from multiple stable isotopes (C, N, Cl) into the photodegradation of herbicides atrazine and metolachlor, *Chemosphere*, 370, 144010, <https://doi.org/10.1016/j.chemosphere.2024.144010>, 2025.
- Liao, Z., Lemke, D., Osenbrück, K., and Cirpka, O. A.: Modeling and inverting reactive stream tracers undergoing two-site sorption and decay in the hyporheic zone, *Water Resour. Res.*, 49, 3406–3422, <https://doi.org/10.1002/wrcr.20276>, 2013.
- 425 Meite, F.: *Transformation et transport des pesticides inorganiques et de synthèse dans les sols de bassins versants agricoles*, Laboratoire d'Hydrologie et de Géochimie de Strasbourg (LHyGeS), l'université de Strasbourg, Strasbourg, 367 pp., 2018.
- NF EN ISO: Method 11369: Water quality — Determination of selected plant treatment agents — Method using high performance liquid chromatography with UV detection after solid-liquid extraction, Association Francaise de Normalisation 19, 1997.
- 430 Payraudeau, S., Alvarez-Zaldivar, P., van Dijk, P., and Imfeld, G.: Constraining topsoil pesticide degradation in a conceptual distributed catchment model with compound-specific isotope analysis (CSIA), *Hydrology and Earth System Sciences*, 29, 4179–4197, <https://doi.org/10.5194/hess-29-4179-2025>, 2025.
- Prueger, J. H., Gish, T. J., McConnell, L. L., McKee, L. G., Hatfield, J. L., and Kustas, W. P.: Solar radiation, relative humidity, and soil water effects on metolachlor volatilization, *Environ. Sci. Technol.*, 39, 5219–5226, <https://doi.org/10.1021/es048341q>, 2005.
- 435 Ramnarine, R., Voroney, R. P., Wagner-Riddle, C., and Dunfield, K. E.: Carbonate removal by acid fumigation for measuring the  $\delta^{13}\text{C}$  of soil organic carbon, *Can. J. Soil Sci.*, 91, 247–250, <https://doi.org/10.4141/cjss10066>, 2011.
- Rice, P. J., Anderson, T. A., and Coats, J. R.: Degradation and persistence of metolachlor in soil: Effects of concentration, soil moisture, soil depth, and sterilization, *Environ. Toxicol. Chem.*, 21, 2640–2648, <https://doi.org/10.1002/etc.5620211216>, 2002.
- 440 Rose, C. E., Coupe, R. H., Capel, P. D., and Webb, R. M. T.: Holistic assessment of occurrence and fate of metolachlor within environmental compartments of agricultural watersheds, *Sci. Total Environ.*, 612, 708–719, <https://doi.org/10.1016/j.scitotenv.2017.08.154>, 2018.

- Salehin, M., Packman, A. I., and Wörman, A.: Comparison of transient storage in vegetated and unvegetated reaches of a small agricultural stream in Sweden: seasonal variation and anthropogenic manipulation, *Adv. Water Resour.*, 26, 951-964, [https://doi.org/10.1016/s0309-1708\(03\)00084-8](https://doi.org/10.1016/s0309-1708(03)00084-8), 2003.
- 445 Schwarzenbach, R. P., Gschwend, P. M., and Imboden, D. M.: *Environmental organic chemistry*, third ed., John Wiley & Sons, 1024 pp.2016.
- Shaw, S. B., Beslity, J. O., and Colvin, M. E.: Working toward a more holistic set of hydrologic principles to teach non-hydrologists: Five simple concepts within catchment hydrology, *Hydrol. Process.*, 33, 2258–2262, <https://doi.org/10.1002/hyp.13485>, 2019.
- Silva, V., Mol, H. G. J., Zomer, P., Tienstra, M., Ritsema, C. J., and Geissen, V.: Pesticide residues in European agricultural soils – A hidden reality unfolded, *Sci. Total Environ.*, 653, 1532–1545, <https://doi.org/10.1016/j.scitotenv.2018.10.441>, 2019.
- 450 Torrentó, C., Ponsin, V., Lihl, C., Hofstetter, T. B., Baran, N., Elsner, M., and Hunkeler, D.: Triple-element compound-specific stable isotope analysis (3D-CSIA): Added value of Cl isotope ratios to assess herbicide degradation, *Environ Sci Technol*, 55, 13891–13901, <https://doi.org/10.1021/acs.est.1c03981>, 2021.
- Van Breukelen, B. M.: Quantifying the degradation and dilution contribution to natural attenuation of contaminants by means of an open system Rayleigh equation, *Environ. Sci. Technol.*, 41, 4980–4985, <https://doi.org/10.1021/es062846u>, 2007.
- 455 Walker, A.: A simulation model for prediction of herbicide persistence, *J. Environ. Qual.*, 3, 396–401, <https://doi.org/10.2134/jeq1974.00472425000300040021x>, 1974.